Day-to-day Variability of Field-Aligned Irregularities Occurrence in Nighttime F-region Ionosphere over the Equatorial Atmosphere Radar: A Combinatorics Analysis

Dyah R. Martiningrum[1,2], Mamoru Yamamoto[1], and Rezy Pradipta[3]

Corresponding author: Rezy Pradipta, Institute for Scientific Research, Boston College, 140 Commonwealth Avenue, Chestnut Hill, MA 02467, USA (rezy.pradipta@bc.edu)

[1]Research Institute for Sustainable Humanosphere (RISH), Kyoto University, Kyoto, Japan

[2]Space Science Center, National Institute of Aeronautics and Space (LAPAN), Bandung, Indonesia

[3]Institute for Scientific Research, Boston College, Chestnut Hill, Massachusetts, USA

Key Points.

- We analyzed the day-to-day variability of field aligned irregularities (FAI) occurrence in nighttime F-region ionosphere over Kototabang
- A statistical combinatorics analysis was used to identify which day-to-day occurrence patterns were dominant during different seasons
- The "combinatorics fingerprints" revealed by the analysis may offer new ways to help forecast FAI occurrence on a regional basis

Abstract. This paper presents a statistical analysis to investigate the day-to-day variability of field-aligned irregularities (FAI) occurrence in nighttime F-region ionosphere over the Equatorial Atmosphere Radar (EAR), West Sumatra, Indonesia. FAI echoes were identified based on signal intensity of backscatter radar observations. We analyzed nighttime F-region FAI during 3 years starting in January 2011 to December 2013. For the first time, a combinatorics analysis was applied to examine the statistical likelihood of various day-to-day FAI occurrence patterns. The empirical day-to-day combinatorics analysis was performed based on binary classification of EAR observation data into either FAI occurrence (+) or absence (-) for each calendar date. Permutations of various day-to-day occurrence patterns, from 1-day to 6-day patterns, were sorted into histograms. The combinatorics analysis was performed in 4 separate time intervals to account for seasonal variation: two equinoxes (March and September) and two solstices (June and December). EAR data show that FAI occurrence probability is maximum for the two equinoxes, and that it is minimum for the two solstices. Our analysis shows that certain day-to-day patterns are more likely to occur than others, and such "combinatorics

fingerprints" depend on season. During the solstices, persistent absence of FAI over several consecutive days far outweighed persistent FAI occurrence over an equivalent grouping of days with the same length. Meanwhile, during the equinoxes, we found a generally more equitable distribution between persistent day-to-day FAI occurrence and persistent day-to-day FAI absence. These findings may open new ways to help forecast FAI occurrence on a regional basis.

1. Introduction

Plasma density irregularities in nighttime low-latitude and equatorial ionosphere, known as equatorial spread-F (ESF) or equatorial plasma bubbles (EPB), occur in a vast range of scale sizes and amplitudes, and can cover a wide range of altitudes, latitudes, and longitude sectors. The formation of ESF/EPB depends on the background ionospheric conditions that determine the growth rate and seeding of the Rayleigh-Taylor instability [e.g. *Kelley*, 2009]. Several ionospheric parameters play key roles in this mechanism. These include the evening prereversal enhancement in vertical plasma drift (PRE), wave structure in plasma density, and electric field polarization to seed the instability. Horizontal geomagnetic field lines at the magnetic equator perpendicular to gravity, prevailing neutral wind, and background electric field are vital factors to the development of such ionospheric plasma density irregularities. Vertical plasma density gradient at the bottomside of ionospheric F-layer is also a significant factor in controlling the growth rate of ESF/EPB. Statistical studies have addressed aspects of ESF/EPB development and occurrence patterns under different geophysical conditions [e.g. *Ogawa et al.*, 2006; *Aswathy and Manju*, 2017; *Yamamoto et al.*, 2018; *Abdu*, 2019] which generally involve major changes in one category of the abovementioned ionospheric parameters at a time.

Large-scale structures of ESF/EPB in general are geomagnetic field aligned. They have zonal (east-west) widths of typically a few tens of km and extend meridionally (north-south) along the geomagnetic field lines for hundreds to thousands of km depending on the apex altitude of the bubbles [e.g. *Sobral et al.*, 2002], while their vertical heights range from a few tens of km to several hundreds of km [e.g. *Labelle et al.*, 1997]. Within the

confine of large-scale plumes of ESF/EPB in the nighttime ionosphere, there are also meter-scale and down to centimeter-scale plasma density irregularities. These interior plasma density irregularities are likewise aligned with the geomagnetic field lines, and they are commonly known as field aligned irregularities (FAI) associated with ESF/EPB. When radio signals propagate through these FAI-filled ionospheric regions, they may experience scintillations. This type of radio wave diffraction-propagation phenomenon results in a fade in the received signal power, which could mean a loss of signal. The region of equatorial scintillations extends 30° latitude on either side of the Earth's magnetic equator and the strongest effects are found around 10°N and 10°S magnetic latitude [e.g. *Wanninger*, 1993].

Variability in the occurrence and severity of ESF/EPB is also present on a wide range of time scales. In multi-year or decadal time scale, long-term variability in the occurrence and severity of ESF/EPB is dependent on the 11-year solar activity cycle. Within each year, the ESF/EPB variability is dependent on the changing season as well as on the systematically varying level of solar flux. Finally, there is variability in terms of the day-to-day occurrence pattern of ESF/EPB. The seasonal variability is relatively better understood and much more predictable, whereas the day-to-day variability is not so easy to predict because of the highly transient nature of the driving sources.

In the present study, we investigated the day-to-day variability of FAI occurrence in nighttime F-region ionosphere over the Sumatra region. The investigation was based on observations by the Equatorial Atmosphere Radar (EAR), and here we introduced the use of statistical combinatorics analysis to keep track of the day-to-day FAI occurrence variability. The combinatorics analysis examines and reveals the existence of day-to-day

occurrence patterns with certain properties. Using such a combinatorics analysis we characterized the patterns of day-to-day FAI occurrence intrinsic to the locally-performed EAR observation data, and established the statistical likelihood for any particular permutation pattern to be followed by another set of permutation pattern in the coming days. In other words, we traced the empirical rules of transformation chain from one permutation pattern into another, as well as sub-configurations of a given permutation pattern. In the following sections below, we provide a general description of the day-to-day combinatorics analysis and discuss the empirical results.

2. Data and Methodology

The Equatorial Atmosphere Radar (EAR) located at Kototabang, West Sumatra, Indonesia (geographic coordinate 0.20°S, 100.32°E; dip latitude 10.36°S) is a large monostatic radar which operates at a frequency of 47.0 MHz. This instrument was developed to study the dynamics of lower and upper atmosphere [*Fukao et.al.*, 2003]. It has a circular antenna array approximately 110 m in diameter and a 3.4° beam width. It also has an active phased-array antenna system, in which each of 560 three-element Yagi antennas is driven by separate solid-state transceiver module. This system configuration allows the radar beam to be steered on a pulse-to-pulse basis up to 5,000 times per second. EAR has been operated to investigate wind, waves, and turbulences in the neutral atmosphere from 1.5 to 20 km altitude (lower atmosphere). For upper atmospheric studies, EAR was primarily designed to be able to receive coherent backscatter echoes from Field Aligned Irregularities (FAI) with 3-meter scale length in the ionospheric E- and F-regions (100–600 km). When operating as a coherent scatter radar as such, EAR needs to point its radar beam in directions perpendicular to the geomagnetic field direction. With the rapid

beam forming and pointing, EAR has a unique capability for surveilling and investigating the spatial structures and temporal variations of ionospheric FAI in different directions simultaneously.

Figure 1 shows a situational map of the geographical region around EAR, along with a conceptual illustration of the routine FAI observations conducted at the radar facility. When FAI are present in the ionosphere, the signal-to-noise ratio (SNR) of backscatter radar echoes will be notably high at the altitude range where the irregularities are. Multi-beam operations with a fan beam configuration (spanning east-west) for these routine FAI observations also help resolve spatial FAI structures and reduce false positive FAI identifications due to instrumental noise in individual radar beams. Since EAR start of operation in 2001, intense FAI echoes had been observed in nighttime ionospheric E- and F-regions over Kototabang. Furthermore, there is also some distinction between post-sunset [e.g. *Huang*, 2018; *Tsunoda et al.*, 2018] and post-midnight FAI [e.g. *Dao et al.*, 2015, 2017; *Otsuka*, 2018] in the continually developing equatorial/low-latitude aeronomy research.

Figure 1

For the purpose of this study, we focused our attention specifically on the nighttime ionospheric F-region FAI, where post-sunset and post-midnight FAI occurrences were bundled as single category. This choice was motivated by practical consideration that ionospheric F-region irregularities, both post-sunset and post-midnight types, are the dominant contributor to disruptions in high-frequency (HF) radio communications in the largely archipelagic Southeast Asia-Pacific region. The investigation was conducted using EAR observation data recorded in 2011–2013, which correspond to the solar maximum phase in Solar Cycle 24. We examined the EAR observation data archive and tabulated a

full list of the calendar dates in 2011–2013 accompanied by their respective classifications: FAI occurrence, FAI no-occurrence, or uncertain (due to missing or incomplete data). The tabulated list of FAI classifications for all examined calendar dates during 2011–2013 are provided in the Supplementary Material. Based on the tabulated list, we subsequently performed the day-to-day combinatorics analysis of nighttime F-region FAI occurrence.

The day-to-day combinatorics analysis can be outlined as follows. In an ideal scenario with no missing data, one may consider the tabulated FAI classifications as a long discrete sequence $\mathcal{S} = \{a_1, a_2, a_3, \ldots, a_N\}$ where a_i is either '+' (representing FAI occurrence) or '−' (representing FAI no-occurrence). Here the index $i = 1, 2, 3, \ldots, N$ signifies the calendar dates arranged in a chronological order. One may then consider a short contiguous chain $\mathcal{K} = \{a_j, a_{j+1}, \ldots, a_{j+k-1}\}$ of length $k \ll N$. The short chain's start index j may vary from 1 to $N - k$. Theoretically, there are 2^k possible unique permutations for such a chain of length k; but only some of these theoretically possible permutations may actually materialize within the empirically-provided $\mathcal{S}$. By sampling the entire long sequence $\mathcal{S}$ (or certain range of $\mathcal{S}$) one would be able to determine which permutations of possible $\mathcal{K}$ actually materialized within $\mathcal{S}$ (or certain range of $\mathcal{S}$). In addition, one would also be able to determine the relative prevalence among the $\mathcal{K}$'s that actually materialized.

In a non-ideal scenario, there would be some missing or incomplete data. In that case, $\mathcal{S} = \{a_1, a_2, a_3, \ldots, a_N\}$ where the element a_i is either '+' (representing FAI occurrence), or '−' (representing FAI no-occurrence), or '?' (representing missing or incomplete data). The combinatorics analysis can still be performed almost exactly like in the ideal case, except that now we shall discard the $\mathcal{K}$'s that contain '?' since they are not very useful to us.

In less abstract terms, the day-to-day combinatorics analysis basically compares the relative prevalence between + and − (1-day patterns $\Leftrightarrow k=1$); between ++, +−, −+, and −− (consecutive 2-day patterns $\Leftrightarrow k=2$); between +++, ++−, +−+, ..., and −−− (consecutive 3-day patterns $\Leftrightarrow k=3$); and so on. For the purpose of the present study, the longest combinatorics under consideration were 6-day patterns ($k=6$). Presented in the next section are the main empirical findings from the investigation.

3. Results and Discussion

Figure 2 shows a plot of FAI occurrence probability over EAR Kototabang based on the 2011–2013 data. The FAI occurrence probability for each day-of-year was determined using a 15-day sliding window (the date in question ±7 days). Based on EAR data that fell within this 15-day date range (selected samples = 3 × 15 = 45 since we used 2011–2013 data), the value of FAI occurrence probability for the date in question is equal to the number of days with FAI occurrence divided by the number of days with valid observations. Calculations were done for all calendar dates from 1 Jan until 31 Dec. Both post-sunset FAI and post-midnight FAI cases were included. The calendar dates were treated as cyclical (31 Dec looped back to 1 Jan), and 29 Feb in a leap year was treated as 1 Mar that happened twice (an extra data sample). Solid black curve on the plot depicts the FAI occurrence probability values obtained from this computation, and dashed gray curves represent 1-sigma binomial proportion confidence interval bounds. Shown on the bottom rows are stem plots of individual FAI occurrences in each year. Blue stems indicate days with FAI occurrence, blank/white spaces indicate days with no occurrence of FAI, and short downward magenta stems indicate days with no (or incomplete) EAR observations.

Figure 2

This FAI occurrence probability curve shows a clear seasonal dependence. Here the FAI occurrence probability reaches maximum around March and September equinoxes; and it is generally lower (or minimum) around June and December solstices. This seasonal pattern is in agreement with the long-term global climatology of equatorial plasma bubbles (EPBs) and scintillations determined from past satellite-borne and ground-based measurements [see e.g. *Aarons*, 1993; *Caton and Groves*, 2006; *Gentile et al.*, 2006a, 2006b; *Comberiate and Paxton*, 2010; *Dao et al.*, 2011; *Yizengaw and Groves*, 2018]. Over EAR Kototabang, the March and September maxima in FAI occurrence probability curve correspond to the time of year when the sunset terminator is aligned with the magnetic meridian, which naturally maximizes the Rayleigh-Taylor instability growth rate that drives the development of EPBs in nighttime ionosphere [see e.g. *Tsunoda*, 1985, 2010].

Following this seasonal pattern, we divided a full year into 4 (four) separate intervals for the purpose of conducting the combinatorics analysis. These designated intervals largely coincide with the two equinoxes and the two solstices. This seasonal partition is indicated by red and green horizontal line segments on the plot in Figure 2. The designated date range for March equinox time period is 15 Feb – 21 May, that for June solstice is 21 May – 20 Aug, that for September equinox is 20 Aug – 15 Nov, and that for December solstice is 15 Nov – 15 Feb. Hence the basic size of these time intervals varied between 88 and 96 days in a year. Note that since we used 3 years worth of EAR data, the total sample size was between 264 and 288 days for each time interval. Depending on the combinatorial length (i.e. 1-day patterns, 2-day patterns ..., or 6-day patterns), we allowed for an additional buffer of up to 5 days at the end of each time interval when performing the day-to-day combinatorics analysis to help smooth out the between-season transition.

Figure 3 shows the results of our day-to-day combinatorics analysis for the March and September equinox time periods, from 1-day patterns to 4-day patterns. The histogram categories include all possible permutations of the day-to-day patterns, where +'s indicate FAI occurrence and −'s indicate FAI no-occurrence. These histograms depict the relative percentage values among categories, with error bars representing theoretical 1-sigma binomial proportion confidence interval. At the most fundamental level, we found that prob(+) > prob(−) in both equinoxes, which is consistent with the empirical fact that FAI occurrence probability reaches maximum during the equinoxes over this geographical location. Looking at the 2-day patterns, we found that prob(++) > prob(+−) and prob(−−) > prob(−+), which indicate that day-to-day persistence tends to prevail during the equinoxes. Looking at the 3-day and 4-day patterns, we found that during the equinoxes the histograms are in the form of a bimodal distribution with major accumulation around persistent FAI occurrence (i.e. consecutive +'s) category and around persistent FAI no-occurrence (i.e. consecutive −'s) category. There is also a minor peak at the center section of the histogram distribution: at categories +−− and −++ among the 3-day patterns for the September equinox, and at category −+++ among the 4-day patterns for both equinoxes. The shape of this minor peak is slightly more symmetrical during the September equinox.

Figure 3

Figure 4 shows the results of our day-to-day combinatorics analysis for the June and December solstice time periods, from 1-day patterns to 4-day patterns. The histograms follow the same format as those shown in Figure 3. Based on the 1-day patterns, we found that prob(−) > prob(+), which is consistent with the empirical fact that FAI occurrence probability reaches minimum during the two solstices over this geographical

Figure 4

location. Unlike the equinoxes, the histograms for the June and December solstices are heavily skewed toward persistent FAI no-occurrence (i.e. consecutive −'s) categories. The histogram readings for persistent FAI occurrence (i.e. consecutive +'s) categories are consistently low during the June and December solstices. Between the two solstices, the skewness of the histogram distribution is much more pronounced during the December solstice.

There are a few notable features that can be discerned from the day-to-day combinatorics patterns depicted in Figures 3 and 4. Most notably, certain day-to-day combinatorics patterns were found to be more dominant, occurring with considerably higher likelihood, than others. The dominant day-to-day patterns (or "winning patterns") were generally different for different seasons of the year. During the two equinoxes, persistent FAI occurrence (i.e. consecutive +'s) patterns were typically the dominant ones — although persistent FAI no-occurrence (i.e. consecutive −'s) patterns were not completely negligible. On the other hand, during the two solstices, persistent FAI no-occurrence (i.e. consecutive −'s) patterns became disproportionately dominant — while persistent FAI occurrence (i.e. consecutive +'s) patterns were virtually nonexistent. This fundamental statistical feature indicates that the geophysical mechanism controlling the day-to-day variability of nighttime FAI is likely not a uniform random process, and it may actually leave some "combinatorics fingerprints" that could be identified in several days of most recent FAI observation history.

Another notable feature from the combinatorics data is that there were certain pairings of day-to-day patterns with consistent statistical equivalency, particularly those asymmetric day-to-day patterns that are mirror image of each other. A case in point here is

the pairing of antisymmetric patterns +− and −+, which consistently had a statistically equivalent likelihood within each of the seasons. We can similarly consider the pairing of antisymmetric patterns +++− and −+++ during both equinoxes, or the pairing of antisymmetric patterns +−− and −−+ (as well as the pairing ++− and −++) during the September equinox, which were in a pairwise statistical tie within their respective domains. Finally, we can also look at the two solstices and consider the pairing of antisymmetric patterns +−− and −−+, or the pairing +−−− and −−−+, or the pairing −+−− and −−+−, which were visibly in a pairwise statistical tie within their respective domains. This particular feature may indicate some kind of time reversibility properties, which are also statistical characteristics shared by certain subset of Markov processes [see e.g. *Kelly*, 1979; *Norris*, 1998]. It therefore suggests that, should the day-to-day variability of nighttime FAI occurrence be modeled using Markov chains, time reversibility properties may have to be placed as major selection criteria.

Figures 5 and 6 show the complete histogram plots of 5-day and 6-day FAI occurrence patterns for all four seasons — March equinox, June solstice, September equinox, and December solstice. The 5-day and 6-day histograms naturally have finer granularity than the 3-day and 4-day histograms, but comparatively lower bin counts and noisier statistics as a consequence. Nevertheless, we found the patterns in the 5-day and 6-day histograms generally consistent with what we have discerned earlier in the 3-day and 4-day histograms. During the solstices, consecutive −'s dominate over every other combinatorial patterns. Meanwhile during the equinoxes, there is a more balanced composition between consecutive +'s and consecutive −'s relative to the rest of the combinatorial patterns. For the benefit of readers at large, full tables of raw histogram counts and percentage values from

Figures 5 and 6

the day-to-day combinatorics analysis (from 1-day to 6-day patterns) in each season are provided in the Supplementary Material.

In addition to examining the prevalence of various day-to-day patterns quantitatively with percentage values (cf. Figures 3–6), we also explored a more qualitative approach for examining the prevalence of day-to-day patterns in terms of their ordinal ranks. The purpose is to elucidate the basic hierarchical structure (i.e. who is number one in terms of prevalence, who are in lower ranks, and who is in the last place) and how the hierarchical status shift between seasons. This topic is discussed below.

Figure 7 depicts a series of line plots showing the rank of each combinatorial pattern during various seasons of the year. For the sake of clarity, here we include only 1-day to 3-day patterns from the combinatorics analysis. Combinatorial pattern with highest histogram count is ranked 1st in its group, and that with lowest histogram count is ranked last in its group. Whenever we have a statistical tie, the pattern listed further up along the y-axis in the standard histograms (cf. Figures 3 and 4) is assigned higher rank. These line plots provide a complementary perspective to the standard histogram plots, showing how each combinatorial pattern either gain or lose rank/dominance as the seasons change. Most prominently, we find that consecutive +'s (i.e. + or ++ or +++ in the plot) are patterns with the most drastic hierarchical gain and loss between consecutive seasons — rapidly switching from the 1st rank to the last rank and vice versa. On the other hand, consecutive −'s (i.e. - or -- or --- in the plot) are the most hierarchically stable patterns — only alternating between the 1st rank to the 2nd rank between seasons. This dynamical tendency further reveals how various day-to-day combinatorial patterns

Figure 7

277 experienced certain shifts in relative hierarchy between seasons, which is a valuable set of
278 information that could be exploited in practical settings.

279 Figure 8 shows a conceptual diagram that illustrates one basic application by which **Figure 8**
280 the results from this day-to-day FAI occurrence combinatorics analysis can be used in
281 practical settings. Given the relative regularity in the seasonal variation of FAI occurrence
282 probability and the unique "combinatorics fingerprints" among various permutations of
283 the day-to-day patterns for each season, an informed estimate on the likelihood of FAI
284 occurrence may be made using past few days of FAI observations (in addition to seasonal
285 climatology). This scheme is quite straightforward to administer, but it contains some
286 inherent limitations in that it may have to be implemented on a regional basis only.
287 The aforementioned regional limitation stems from the prospect that the combinatorics
288 fingerprints may not be universally transferrable to other longitude sectors. Nonetheless,
289 with such a scheme, one may be able to start estimating the local FAI occurrence likelihood
290 12–24 hours in advance of its onset time. Additional set of preparations specific to the
291 desired operational area would be necessary in order to suppress statistical uncertainties
292 as much as possible. This regional scheme may be used in conjunction with a number of
293 other methods for forecasting the occurrence of EPBs, spread-F, and scintillations [e.g.
294 *Secan et al.*, 1995; *Groves et al.*, 1997; *Redmon et al.*, 2010; *Carter et al.*, 2014a, 2014b;
295 *Anderson and Redmon*, 2017].

4. Conclusion

296 We have analyzed the day-to-day variability of FAI in nighttime F-region ionosphere
297 based on observations using EAR at Kototabang, Indonesia. Specifically, we applied a
298 combinatorics analysis on EAR FAI data collected during 2011-2013, including both post-

sunset and post-midnight FAI occurrences. The introduction of combinatorics analysis in the present work allowed us to thoroughly examine the day-to-day variability of FAI occurrence without explicit need for external reference to potential drivers in the solar wind or in the lower atmosphere. Our findings can be summarized as follows: (1) Certain combinatorial patterns were found to be more dominant, i.e. occurring with considerably higher likelihood, than others. (2) The likelihood and ordinal ranks of various combinatorial patterns generally varied with season. (3) Certain pairings of those combinatorial patterns indicate some kind of time reversibility property, a statistical characteristics also shared by certain subset of Markov processes. (4) Patterns revealed by the analysis constitute a form of "combinatorics fingerprints" characterizing the region/season, which may offer some new ways of forecasting FAI on a regional basis.

Acknowledgments. The EAR is operated by the Research Institute for Sustainable Humanosphere (RISH), Kyoto University, and the Indonesian National Institute of Aeronautics and Space (LAPAN). This work was also supported by RISET-Pro Scholarship Program from Ministry of Research and Technology/National Agency for Research and Innovation of Indonesia. Datafiles and summary plots of EAR observations are available from `http://www2.rish.kyoto-u.ac.jp/ear/data-fai/index.html`.

References

Aarons, J. (1993), The longitudinal morphology of equatorial F-layer irregularities relevant to their occurrence, *Space Sci. Rev.*, 63, 209.

Abdu, M.A. (2019), Day to day and short-term variabilities in the equatorial plasma bubble/spread F irregularity seeding and development, *Progress in Earth and Planetary*

Science, doi/;10.1186/s40645-019-0258-1.

Anderson, D. N., and R. J. Redmon (2017), Forecasting scintillation activity and equatorial spread F, *Space Weather*, 15, 495-502, doi:10.1002/2016SW001554.

Aswathy, R.P., and G. Manju (2017), Gravity wave control on ESF day to day variability: an empirical approach, *J. Geophys. Res. Space Physics*, 122, 6791-6798, doi: 10.1002/2017JA023983.

Carter, B. A., et al. (2014a), Geomagnetic control of equatorial plasma bubble activity modeled by the TIEGCM with Kp, *Geophys. Res. Lett.*, 41, 5331-5339, doi:10.1002/2014GL060953.

Carter, B. A., et al. (2014b), Using solar wind data to predict daily GPS scintillation occurrence in the African and Asian low-latitude regions, *Geophys. Res. Lett.*, 41, 8176-8184, doi:10.1002/2014GL062203.

Caton, R., and K. M. Groves, (2006), Longitudinal correlation of equatorial ionospheric scintillation, *Radio Sci.*, 41, RS5S22, doi:10.1029/2005RS003357.

Comberiate, J., and L. J. Paxton (2010), Global Ultraviolet Imager equatorial plasma bubble imaging and climatology, 2002-2007, *J. Geophys. Res.*, 115, A04305, doi:10.1029/2009JA014707.

Dao, E., M. C. Kelley, P. Roddy, J. Retterer, J. O. Ballenthin, O. de La Beaujardiere, and Y.-J. Su (2011), Longitudinal and seasonal dependence of nighttime equatorial plasma density irregularities during solar minimum detected on the C/NOFS satellite, *Geophys. Res. Lett.*, 38, L10104, doi:10.1029/2011GL047046.

Dao, T, Y. Otsuka, K. Shiokawa, S. T. Ram, and M. Yamamoto (2015), Altitude development of postmidnight F region field-aligned irregularities observed us-

ing Equatorial Atmosphere Radar in Indonesia, *Geophys. Res. Lett.*, 43, 1015-1022, doi:10.1002/2015GL067432.

Dao, T., Y. Otsuka, K. Shiokawa, M. Nishioka, M. Yamamoto, S. M. Buhari, M. Abdullah, and A. Husin (2017), Coordinated observations of postmidnight irregularities and thermospheric neutral winds and temperatures at low latitudes, *J. Geophys. Res. Space Physics*, 122, 7504-7518, doi:10.1002/2017JA024048.

Fukao, S., H. Hashiguchi, M. Yamamoto, T. Tsuda, T. Nakamura, M.K. Yamamoto, T. Sato, M. Hagio, Y. Yabugaki (2003), Equatorial Atmosphere Radar (EAR): System description and first results, *Radio Science*, 38(3), 1053, doi:10.1029/2002RS002767.

Gentile, L. C., W. J. Burke, and F. J. Rich (2006a), A global climatology for equatorial plasma bubbles in the topside ionosphere, *Ann. Geophys.*, 24, 163.

Gentile, L. C., W. J. Burke, and F. J. Rich (2006b), A climatology of equatorial plasma bubbles from DMSP 1989-2004, *Radio Sci.*, 41, RS5S21, doi:10.1029/2005RS003340.

Groves, K. M., et al. (1997), Equatorial scintillation and systems support, *Radio Sci.*, 32(5), 2047-2064, doi:10.1029/97RS00836.

Huang, C. S. (2018), Effects of the postsunset vertical plasma drift on the generation of equatorial spread F, *Prog. Earth Planet. Sci.*, 5(3), doi:10.1186/s40645-017-0155-4.

Kelley, M.C. (2009), The Earth's ionosphere: plasma physics and electrodynamics, 2nd edn., *Academic Press*, Amsterdam.

Kelly, F. (1979), Reversibility and Stochastic Networks, *Wiley*, 1979.

Labelle, J., J. M. Jahn, R. F. Pfaff, W. E. Swartz, J. H. A. Sobral, M. A. Abdu, P. Muralikrishna, and E. R. de Paula (1997), The Brazil/Guara equatorial spread F campaign: results of the large-scale measurements, *Geophys. Res. Lett.*, 24(13), 1691-1694.

366 Norris, J. R. (1998), Markov Chains, *Cambridge University Press*, 1998.

367 Ogawa, T., Y. Otsuka, K. Shiokawa, A. Saito, M. Nishioka (2006), Ionospheric distur-
368 bances over Indonesia and their possible association with atmospheric gravity waves
369 from the troposphere, *Journal of The Meteorological Society of Japan*, Vol. 84A, pp.
370 327-342.

371 Otsuka, Y. (2018), Review of the generation mechanisms of post-midnight irregulari-
372 ties in the equatorial and low-latitude ionosphere, *Prog. Earth Planet. Sci.*, 5(57),
373 doi:10.1186/s40645-018-0212-7.

374 Redmon, R. J., D. Anderson, R. Caton, and T. Bullett (2010), A Forecast-
375 ing Ionospheric Real-time Scintillation Tool (FIRST), *Space Weather*, 8, S12003,
376 doi:10.1029/2010SW000582.

377 Secan, J. A., R. M. Bussey, E. J. Fremouw, and S. Basu (1995), An improved model of
378 equatorial scintillation, *Radio Sci.*, 30(3), 607-617, doi:10.1029/94RS03172.

379 Sobral, J. H. A., M. A. Abdu, H. Takahashi, M. J. Taylor, E. R. de Paula, C. J. Zamlutti,
380 M.G. de Aquino, and G. L. Borba (2002), Ionospheric plasma bubble climatology over
381 Brazil based on 22 years (1977-1998) of 630 nm airglow observations, *J. Atmos. Terr.*
382 *Phys.*, 64, 1517-1524.

383 Tsunoda, R. T. (1985), Control of the seasonal and longitudinal occurrence of equatorial
384 scintillations by the longitudinal gradient in integrated E region Pedersen conductivity,
385 *J. Geophys. Res.*, 90 (A1), 447-456, doi:10.1029/JA090iA01p00447.

386 Tsunoda, R. T. (2010), On seeding equatorial spread F during solstices, *Geophys. Res.*
387 *Lett.*, 37, L05102, doi:10.1029/2010GL042576.

388 Tsunoda, R. T., S. Saito, and T. T. Nguyen (2018), Post-sunset rise of equatorial F layer–
389 or upwelling growth?, *Prog. Earth Planet. Sci.*, 5(22), doi:10.1186/s40645-018-0179-4.
390 Wanninger, L. (1993), Effects of the Equatorial Ionospheric on GPS, *GPS World* July
391 1993, p. 48-54.
392 Yamamoto, M., Y. Otsuka, H. Jin, Y. Miyoshi (2018), Relationship between day-to-day
393 variability of equatorial plasma bubble activity from GPS scintillation and atmospheric
394 properties from Ground-to-topside model of Atmosphere and Ionosphere for Aeronomy
395 (GAIA) assimilation, *Progress in Earth and Planetary Science*, doi:10.1186/s40645-018-
396 0184-7.
397 Yizengaw, E., and K. M. Groves (2018), Longitudinal and seasonal variability of equa-
398 torial ionospheric irregularities and electrodynamics, *Space Weather*, 16, 946-968,
399 doi:10.1029/2018SW001980.

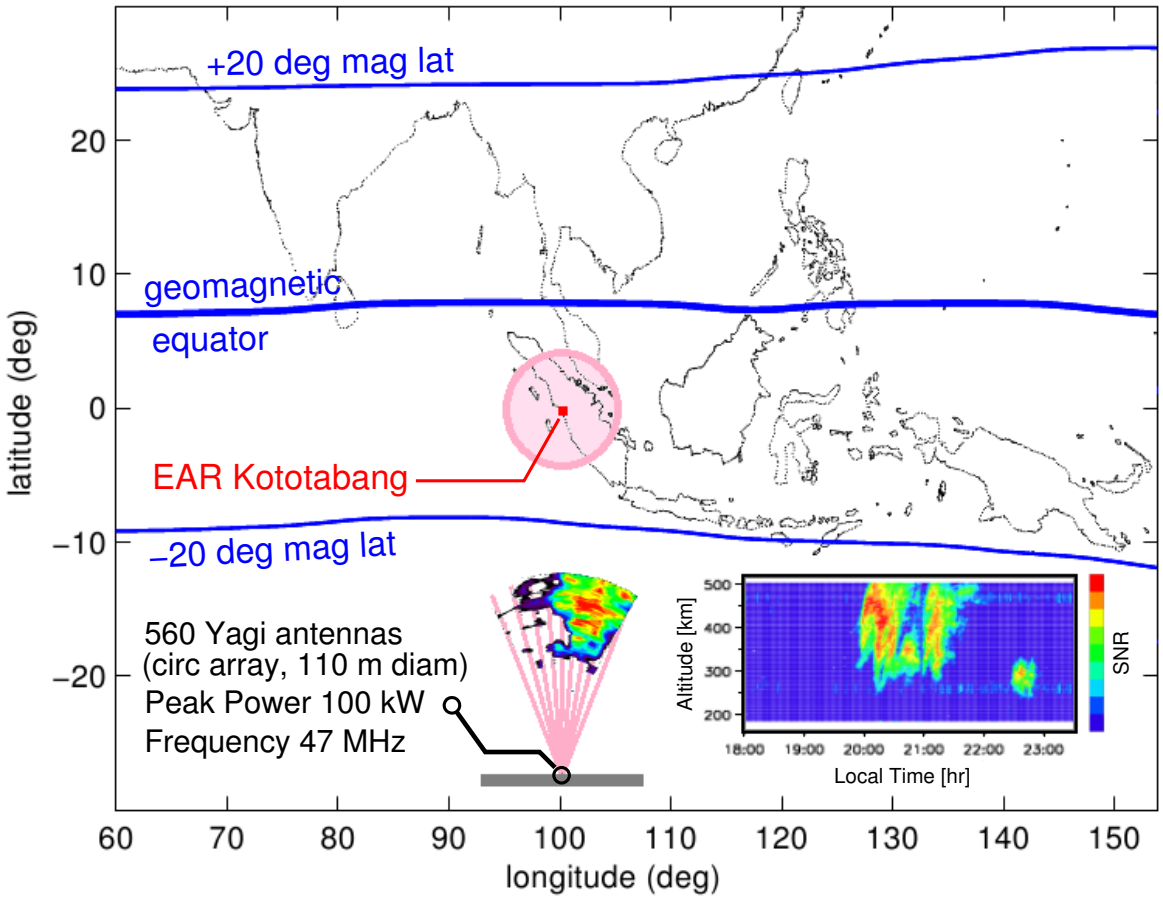

Figure 1. A situational map of geographic area around EAR Kototabang. The geomagnetic equator and $\pm 20^\circ$ magnetic latitude lines are shown as solid blue curves, the EAR site is marked with a red square, and the theoretically possible EAR coverage at ionospheric F-region altitude is indicated by shaded circle. Also shown illustratively are the typical EAR fan beam configuration (spanning west-east) and a sample range-time-intensity (RTI) plot of radar backscatter power with return echoes from FAI.

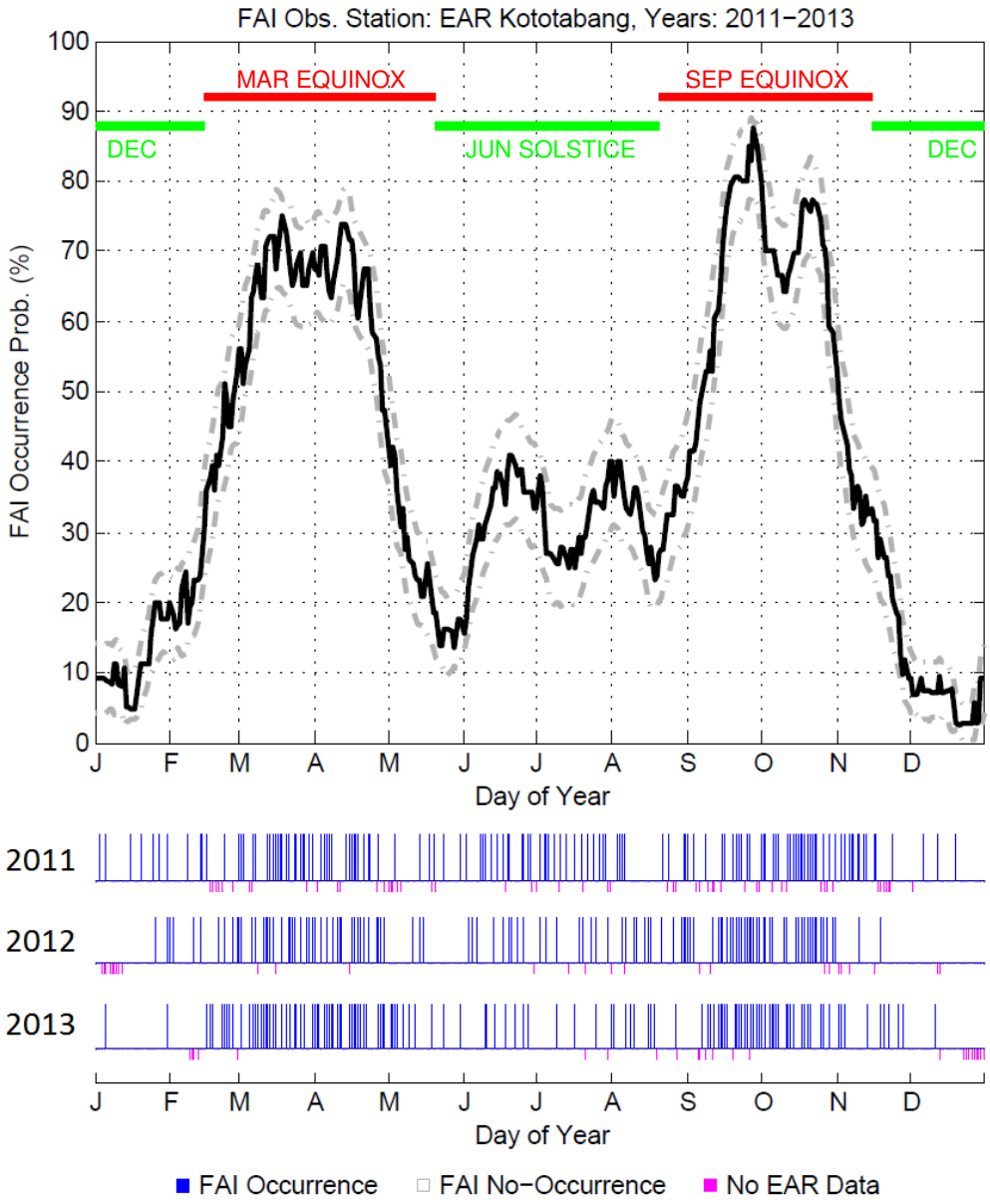

Figure 2. Probability of nighttime ionospheric F-region FAI occurrence over Kototabang as a function of season (day-of-year), derived from the 2011–2013 EAR data. Time intervals associated with the equinoxes and solstices, constructed as partition windows for the combinatorics analysis, are indicated by red and green horizontal line segments on the plot. Shown on the bottom rows are the corresponding stem plots of those nighttime F-region FAI occurrences individually in each year.

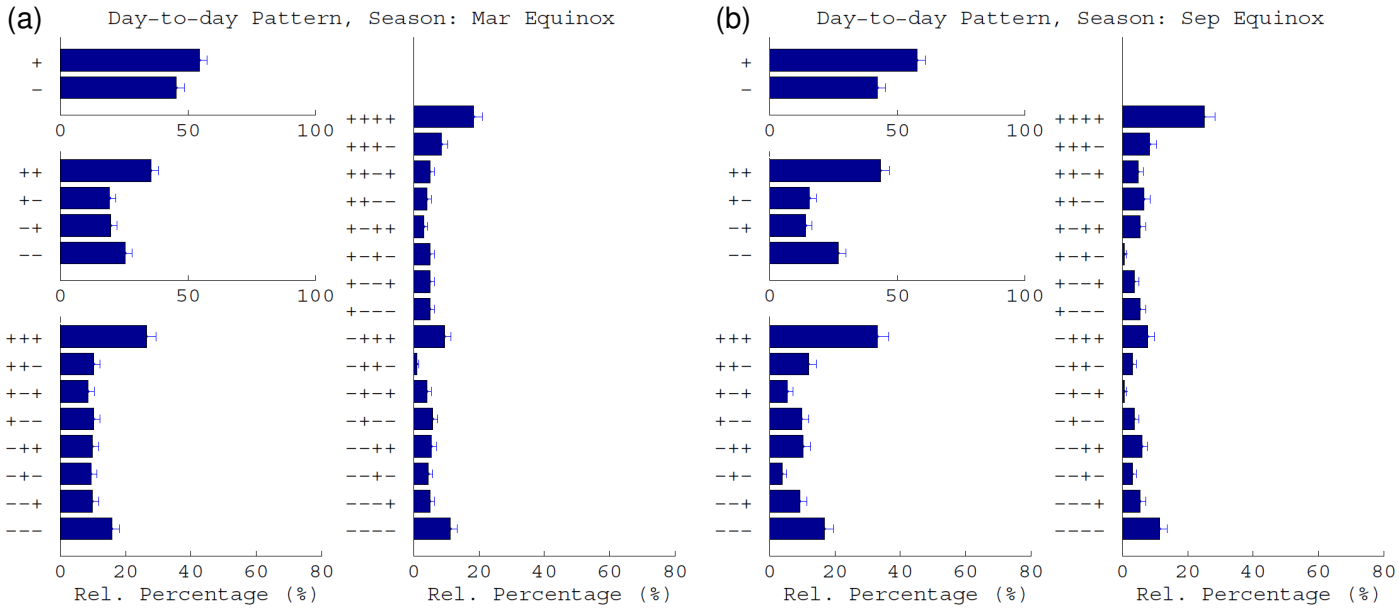

Figure 3. Histograms of various day-to-day combinatorial patterns of nighttime ionospheric F-region FAI occurrence over Kototabang, based on 2011–2013 EAR observations around the equinoxes — when the seasonal FAI occurrence probability at this longitude sector is maximum. (a) Combinatorial patterns for March equinox, and (b) for September equinox.

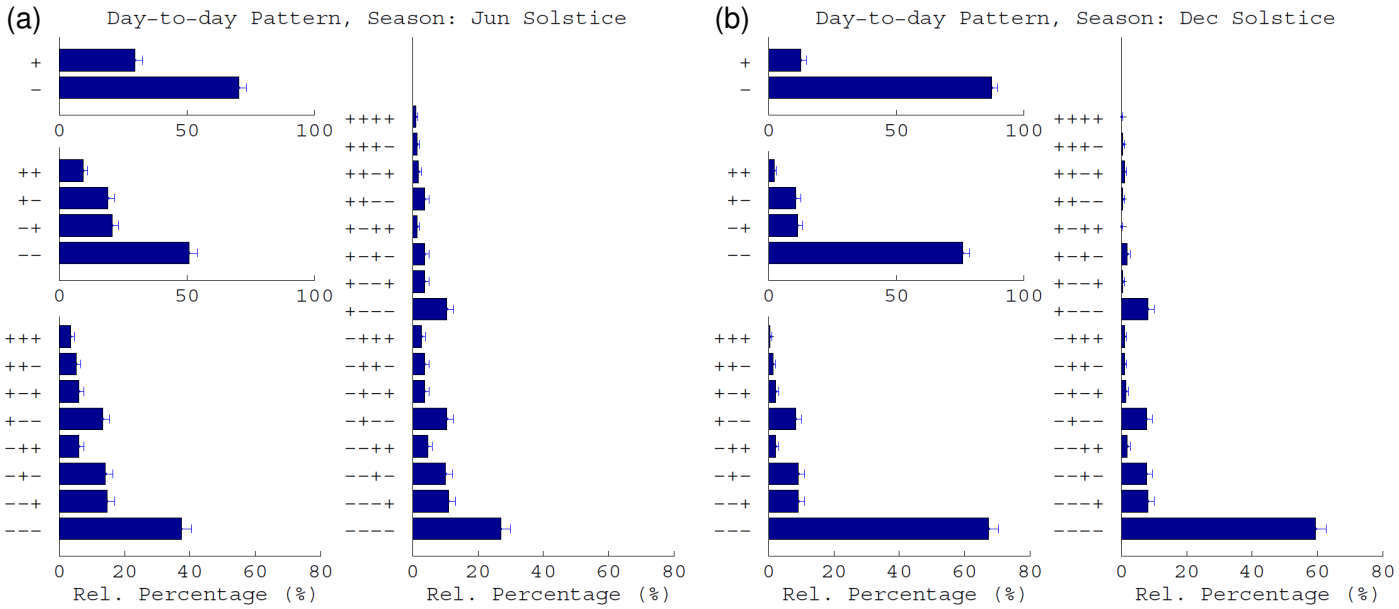

Figure 4. Histograms of various day-to-day combinatorial patterns of nighttime ionospheric F-region FAI occurrence over Kototabang, based on 2011–2013 EAR observations around the solstices — when the seasonal FAI occurrence probability at this longitude sector is minimum. (a) Combinatorial patterns for June solstice, and (b) for December solstice.

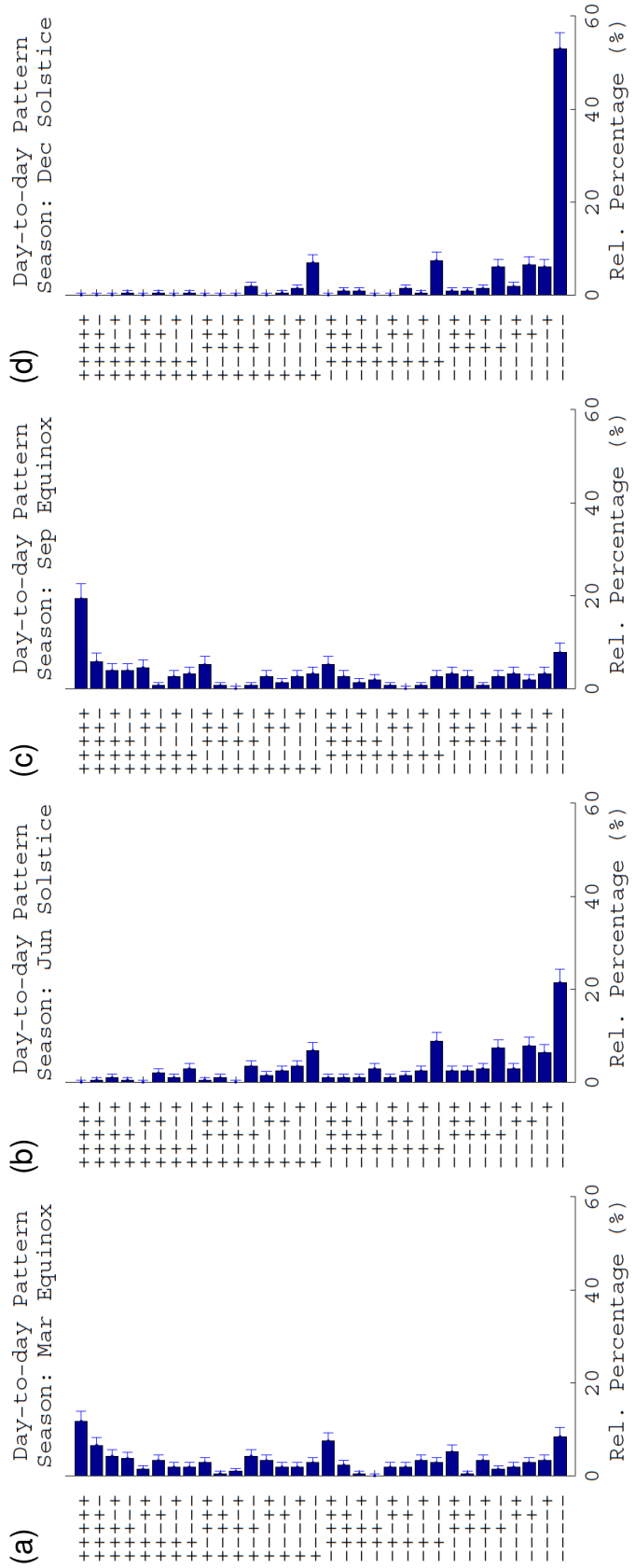

Figure 5. A full overview of 5-day combinatorial pattern histograms of nighttime ionospheric F-region FAI occurrence over Kototabang from 2011–2013 EAR observations for (a) March equinox, (b) June Solstice, (c) September equinox, and (d) December solstice.

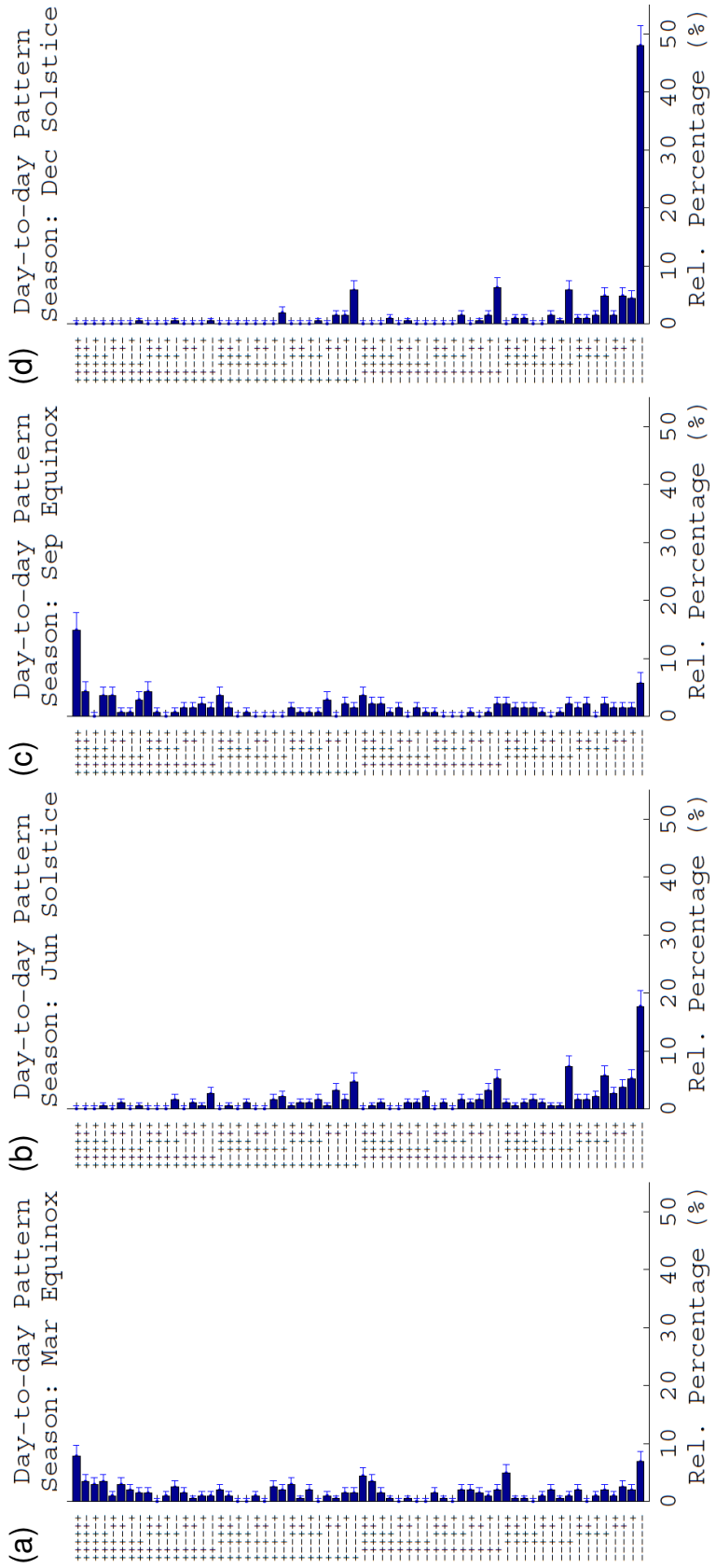

Figure 6. A full overview of 6-day combinatorial pattern histograms of nighttime ionospheric F-region FAI occurrence over Kototabang from 2011–2013 EAR observations for (a) March equinox, (b) June Solstice, (c) September equinox, and (d) December solstice.

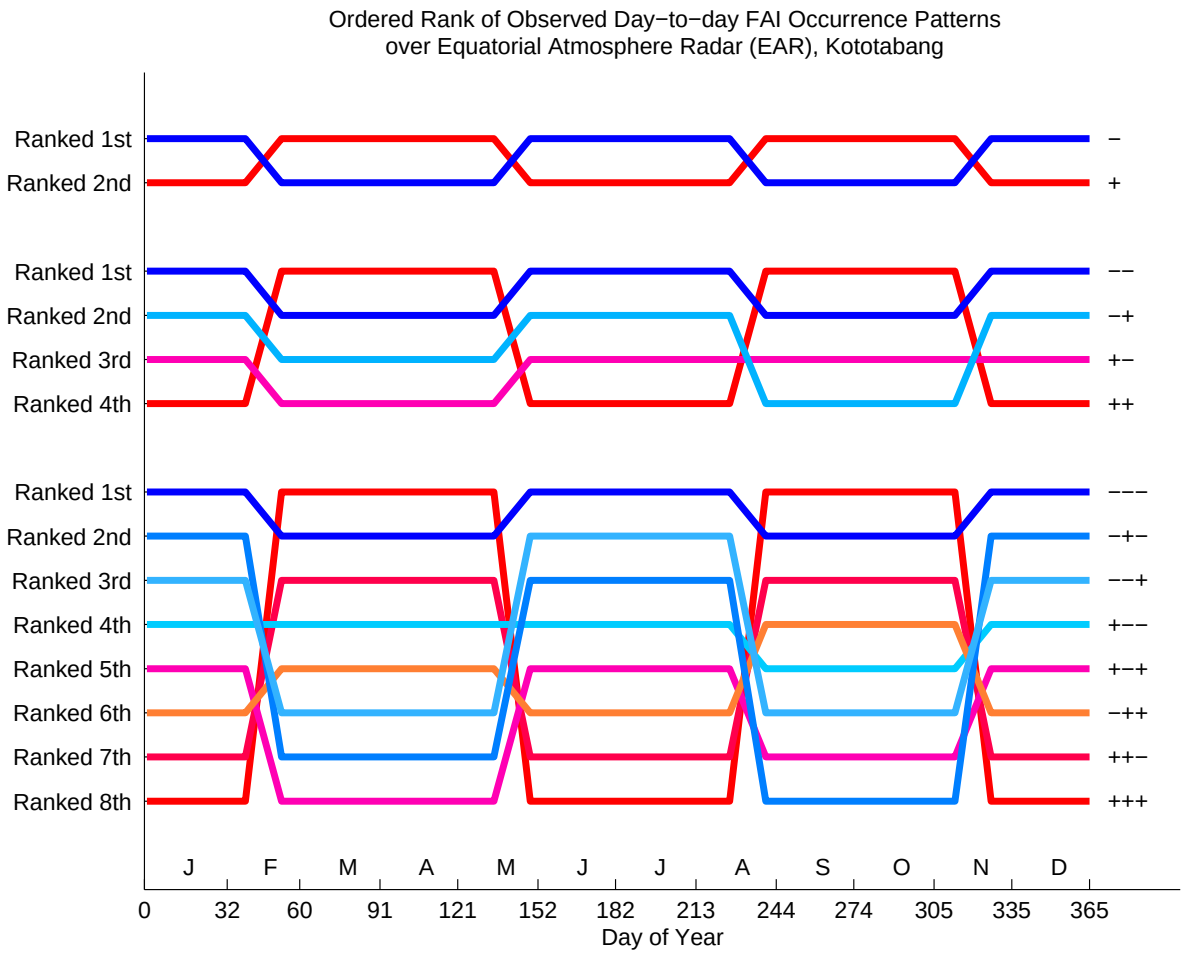

Figure 7. Ordered rank of various combinatorial patterns during different seasons of the year. The top cluster of curves show the seasonal evolution of attained ranks for the 1-day patterns, middle cluster for the 2-day patterns, and bottom cluster for the 3-day patterns.

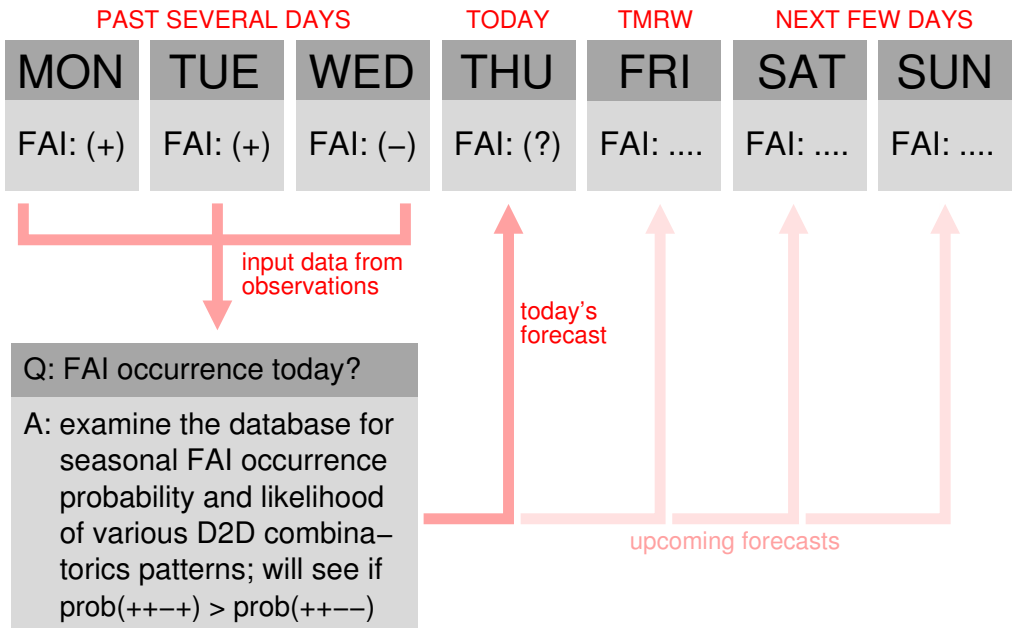

Figure 8. Potential utilization of accumulated statistical results from the day-to-day (D2D) combinatorial analysis, in practical settings, to help forecast the occurrence probability of nighttime FAI 12–24 hours in advance.